PROCESSING GROUND PENETRATING RADAR DATA TO IMPROVE RESOLUTION OF NEAR-SURFACE TARGETS

by
Kevin Gerlitz[1], Michael D. Knoll[1], Guy M. Cross[2]
Robert D. Luzitano[2] and Rosemary Knight[1,2]

[1]Department of Geological Sciences
[2]Department of Geophysics and Astronomy
129 - 2219 Main Mall
University of British Columbia
Vancouver, British Columbia, V6T 1Z4

ABSTRACT

Although unprocessed ground penetrating radar (GPR) data are capable of producing detailed images of the shallow subsurface, these images may be difficult to interpret reliably. Here, we investigate characteristics of GPR signals and various techniques to enhance GPR images. The processing steps are tested on GPR datasets acquired at a well-controlled site where two concrete blocks, simulating archaeological structures, are buried less than two meters from the surface.

Short range GPR signals often possess a low-frequency component (commonly referred to as a "wow") that causes amplitude distortion along an individual trace. Characteristics of this noise are considered in light of its physical cause, i.e., saturation of the receiver electronics. Three filter techniques were tested to remove the wow: (i) residual mean filtering, (ii) bandpass filtering, and (iii) residual median filtering. We found that the residual median filter performed best. Additional signal processing steps included static corrections, normal moveout (NMO) corrections, migration and eigen filtering. Static corrections compensate for drift of the time-zero sample that occurs during acquisition. NMO corrections remove spatial distortion due to source-receiver offset. Migration focuses diffracted energy and corrects dipping reflectors thereby improving spatial resolution. Eigen filtering removes the coherent direct arrivals to improve the detection of near-surface features.

Application of these processing techniques significantly improves the quality of the GPR images from the test site, both in terms of the positioning of events and resolving capability. By testing various enhancement techniques on data collected at well-controlled sites, a better understanding is gained of their relative benefits and the ultimate capabilities of GPR as a shallow exploration tool.

INTRODUCTION

Like the seismic reflection method, the ground penetrating radar (GPR) technique relies on the propagation of waves in the subsurface and the partial reflection of these waves whenever a contrast in physical properties is encountered. While seismic methods employ elastic waves, GPR utilizes electromagnetic (EM) waves. This similarity allows GPR data to be treated using conventional seismic processing software.

The processing of GPR data has recently been addressed by several authors including Inkster et al. (1989) and Fisher et al. (1992). These papers demonstrate the applicability of seismic processing techniques to image the subsurface at depths greater than a few meters. However, little work has been done on the problem of GPR images at shallower depths. This paper addresses this problem and tests conventional processing techniques on a GPR dataset collected at a well-controlled site. Processing was accomplished with the Inverse Theory & Applications (IT&A), Inc. seismic signal processing software and with routines written by the authors.

SITE DESCRIPTION AND DATA ACQUISITION

The pulseEKKO IV GPR system manufactured by Sensors and Software, Inc., was used for the surveys. The surveys were conducted at a shallow geophysical test site located on the University of British Columbia campus. The site consists of a pit with two concrete blocks placed on excavated clay ledges, at depths of approximately 1 m and 2 m, and back-filled with a coarse-grained, homogeneous sand. A photograph of the pit is shown in Figure 1. The dimensions of the shallow and deep blocks are 150 cm x 40 cm x 50 cm and 150 cm x 60 cm x 50 cm, respectively. The dimensions of the pit and the positions of the blocks are shown in the map and cross-sectional views of Figure 2.

The data consist of common-offset profiles and common-midpoint gathers, each acquired with 100 MHz and 200 MHz antennas. The common offset profiles are 10.9 m long with a station interval of 0.05 m and a constant antenna offset of 0.60 m, yielding two radar profiles of 218 traces of 127.2 ns duration. Common midpoint gathers were centered over the shallow block at 3.18 m (position shown in Figure 2) with an offset increment of 0.04 m. The gathers consist of 74 traces of 127.2 ns duration.

In the unprocessed 100 MHz profile (Figure 3), the direct air and ground waves are evident as the strong events that occur between 0.010 μs and 0.040 μs. Notice also the gradual decrease of the first break arrival time, from 0.015 μs in the leftmost trace to 0.011 μs in the rightmost trace. The clay ledge, upon which the shallow block lies, appears as the strong linear reflector at 0.049 μs between 2.0 m and 4.5 m. The top of the deep block appears at 0.058 μs between 4.9 m and 6.5 m and is associated with distinct diffractions from its edges. The base of the deep block is difficult to see due to the interfering effects of diffractions from various corners and edges. The sloping pit wall is seen as the event having its onset at 7.75m and dipping towards the lower

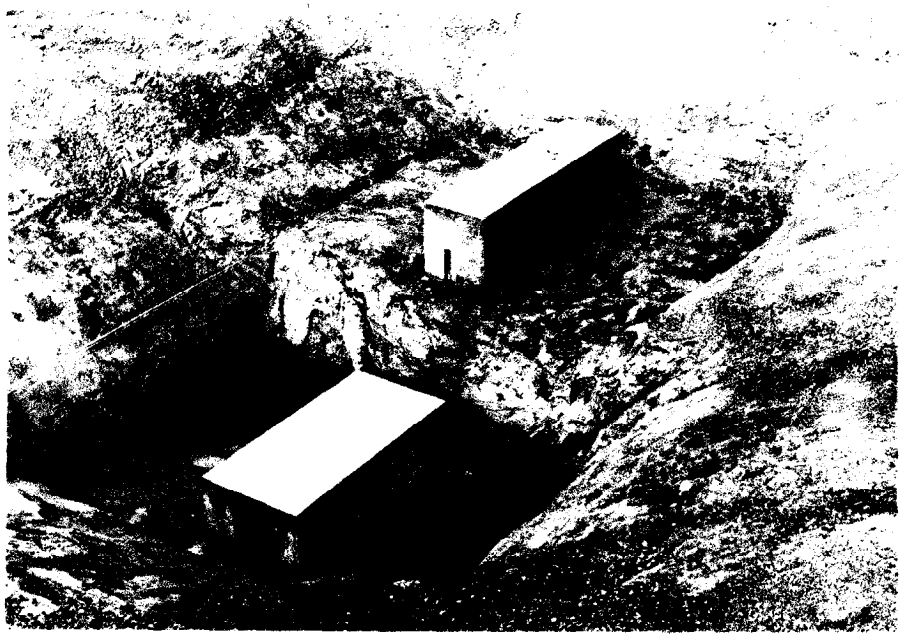

Figure 1: Photograph of test pit with deep block in foreground. Note the hammer resting against the shallow block for scale.

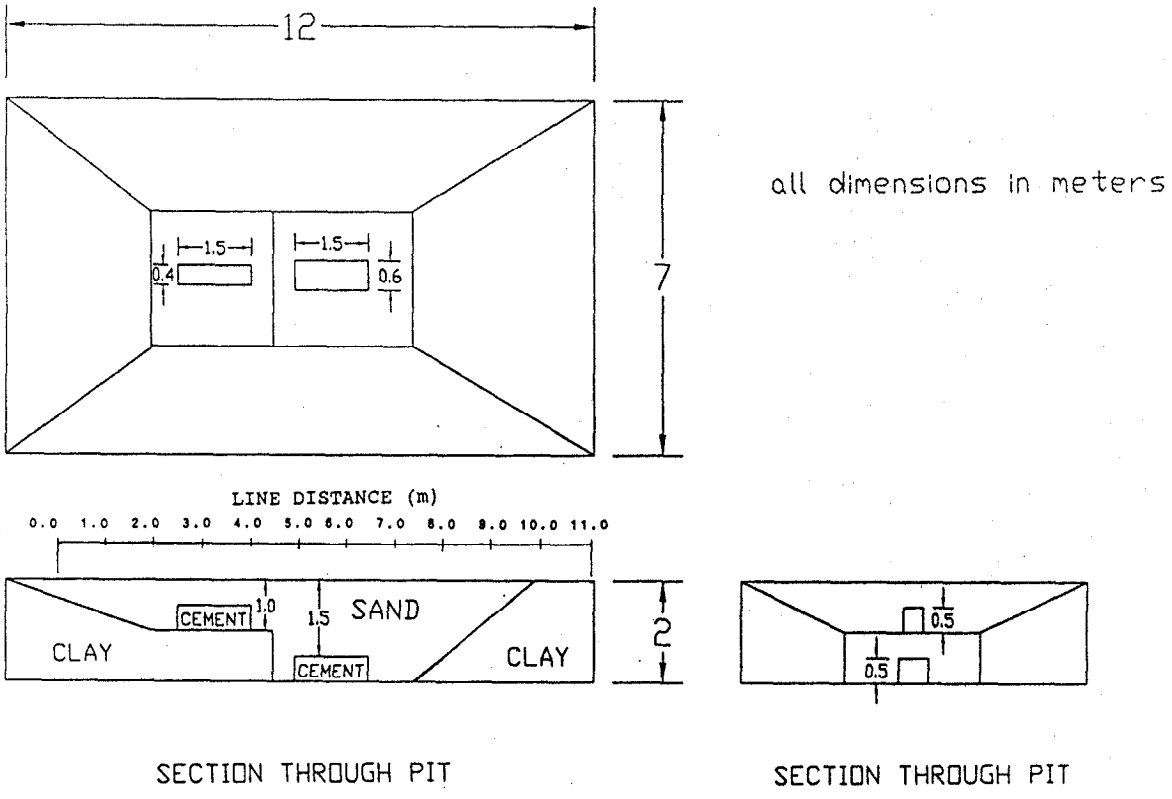

Figure 2: Map and cross-sectional views of test pit. Dimensions and positions of the blocks are accurate to 1 cm.

middle part of the profile. Note also the predominance of black shading in the lower portion of the profile. This indicates that all the traces are biased towards positive values. The 200 MHz profile has many of the traits of the 100 MHz profile, but also includes a weak reflection from the top of the shallow block. This weak near-surface reflector is partially obscured by strong direct arrivals.

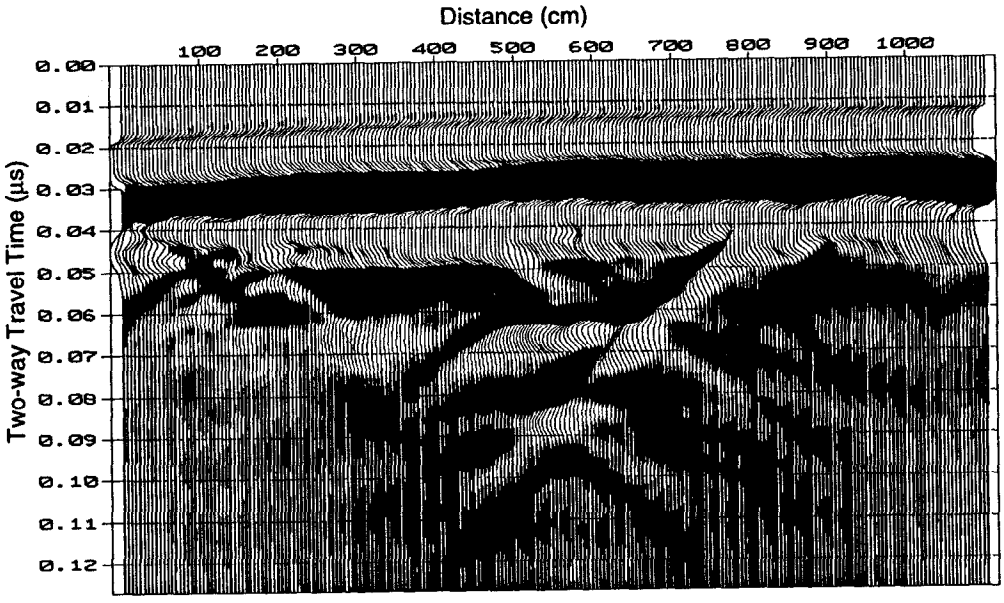

Figure 3: 100 MHz common-offset profile

DATA PRECONDITIONING

Every unprocessed radar trace contains an inherent "wow". The "wow" is due to the saturation of the receiver electronics by the very high amplitude signal, i.e., air-ground pulse interference. The wow is characterized by having a sharp onset to a maximum value (i.e., an edge) then decaying exponentially. This results in a trace that consists of both a "wow" component and a "signal" component as shown in Figure 4.

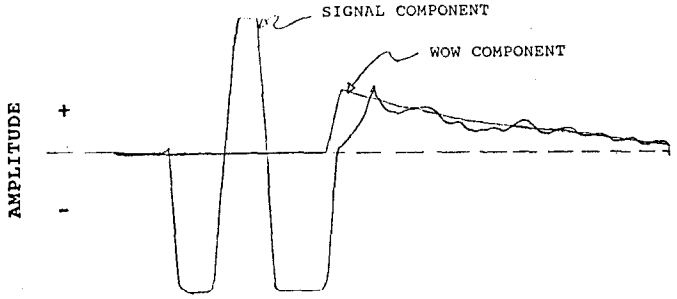

Figure 4: Signal and wow components of an unprocessed radar trace

The result of the "wow" in the signal is to skew traces more positive than negative (or vice versa) so that the traces have non-zero mean (as shown by the 100 MHz profile in Figure 3). Removal of the wow should be done to create a zero-mean trace and thus make the small amplitudes of the signal component more distinct. This can be accomplished by several methods:

(1) residual mean filtering,
(2) bandpass filtering,
(3) residual median filtering.

Residual Mean Filtering

One method often used for wow-removal involves the use of a residual running mean filter. The mean filters consisted of a 25-point window and a 13-point window for the 100 and 200 Mhz datasets, respectively. The residual filtered trace is obtained by subtracting the filtered data from the raw data. A comparison of the residual mean filtered data and the raw data is shown in Figure 5. Although the residual mean filter creates a zero-mean trace, artifacts due to the smoothing properties of the filter are also present. The roughness and the extra lobes of the residual trace are due to the inability of the mean to preserve edges. When the mean trace is subtracted from the raw data trace, the high frequencies associated with edges remain.

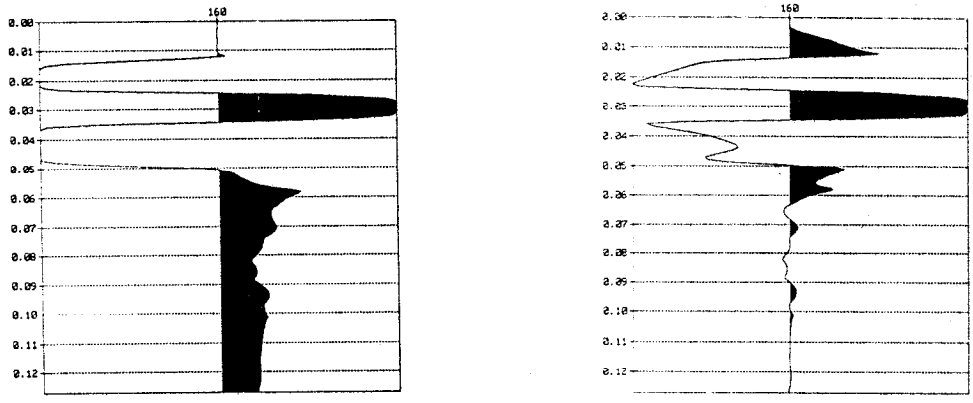

Figure 5: Comparison of an unprocessed radar trace before (left) and after (right) residual mean filtering.

Bandpass Filtering

The conventional approach towards removal of unwanted low frequency noise is high pass filtering. Typically, the dominant frequency range of the wow appears as a prominent peak at the low end of the amplitude spectra. Figure 6 illustrates the wow's spectral signature, especially evident in a CMP where the wow component quickly decreases with increasing offset while the signal

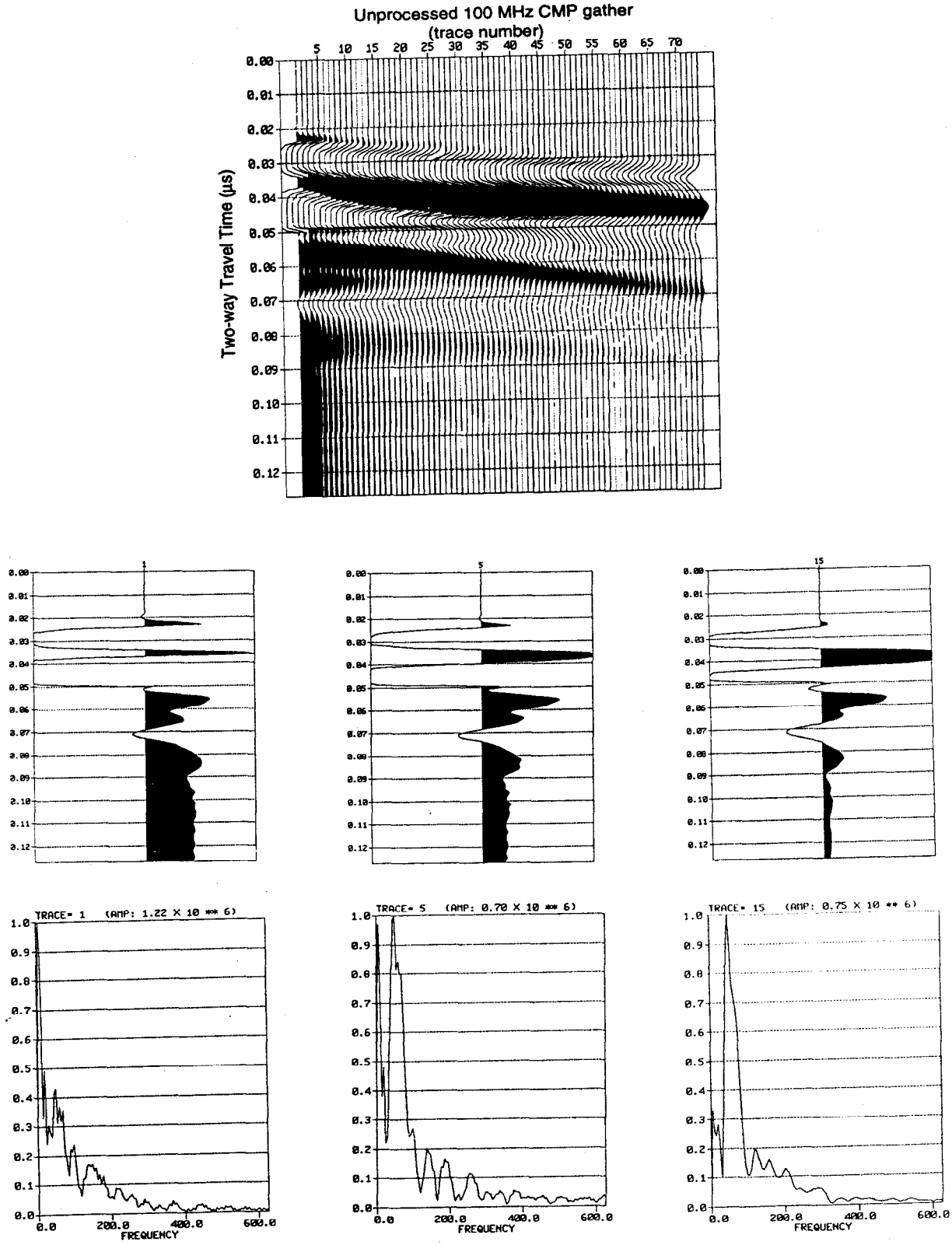

Figure 6: 100 MHz CMP gather and associated amplitude spectra

component remains relatively constant. A 20-500 MHz bandpass filter was applied to the 100 MHz data and a comparison is shown in Figure 7. As seen in Figure 7, the filter was less successful in removing the wow and also produced some artifacts from the filtering process. The inability to completely filter out the wow is due to its frequency content not being limited to the range identifiable in the spectra. The wow also contains significant energy within the signal range. The bandpass filter simply passes the wow component with frequencies between 20 MHz and 500 MHz.

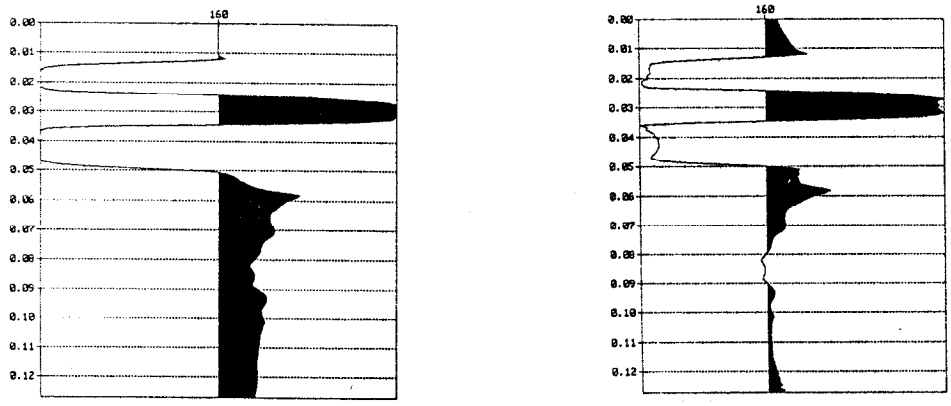

Figure 7: Comparison of an unprocessed radar trace (left) with a bandpass (20-500 MHz) filtered trace (right).

Residual Median Filtering

The running median filter possesses robust properties, well suited to extracting slowly varying signals while preserving edges. Usually, the window length of a median filter is written as (2n+1), where n is a real integer. The median filter is usually used as a filter for removing spurious noise and leaving a signal which is monotonic for n points (Nodes and Gallagher, 1982). Residual median filtering removes gross structure (in this case, the wow) and leaves the smaller reflections intact (Clarke, 1989).

Commonly, median filter lengths are selected by a trial-and-error procedure, comparing the filter's output with the input until the desired result is achieved. Instead, we utilized the amplitude spectra of the radar traces to derive the median filter window length. As seen in Figure 6, the peak associated with the low frequency wow and the peak associated with the dominant signal component are often distinctly separated by a trough. The frequency at which the trough converges is assumed to be an appropriate choice for a cutoff frequency. The corresponding cut-off period is divided by the sampling interval to yield the associated number of data points. This number is equal to n+1 (since median filtering removes blocks of length n) and thus an

appropriate filter length of 2n+1 can be derived (see Figure 8 for a sample calculation).

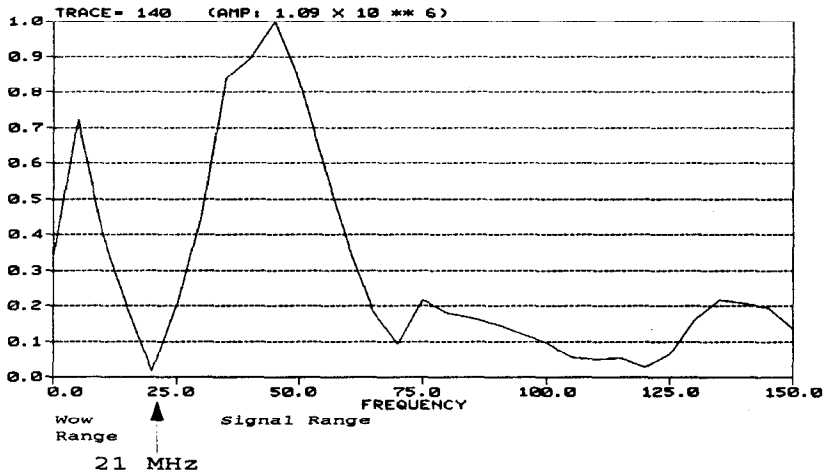

Period, T = 1/f = 1/(21 MHz) = 47.62 ns
Sampling interval = 0.8 ns/point
Number of points = (47.62 ns)/(0.8 ns/pt) = 59 points
n + 1 = 59
n = 58
Median filter window length = (2n+1)= 117

Figure 8: Sample calculation for deriving median filter window length.

A common-offset profile will yield a variety of possible cut-off values. Choosing a filter length smaller than the wow cut-off length will result in the loss of some of the signal to the median trace. Similarly, a filter longer than that derived from the wow cut-off length will result in the contamination of the residual traces with wow. This requires that either each trace be individually filtered with its own appropriate filter length or that an average filter length be applied. An average filter length is usually very effective. Occasionally different filter lengths may be required in association with lateral variations in the electrical properties of the subsurface. Average filter lengths of 117 points and 85 points were used for the 100 MHz and the 200 MHz data, respectively. To permit filtering an entire trace, n data points equal to the first and last datum values are appended to the beginning and end of the trace, respectively. The appended values are removed after filtering to yield a trace which is the same length as the original. A comparison of the unprocessed trace versus the residual median trace is shown in Figure 9. This technique is superior for retaining the true characteristics of the signal while effectively removing wow.

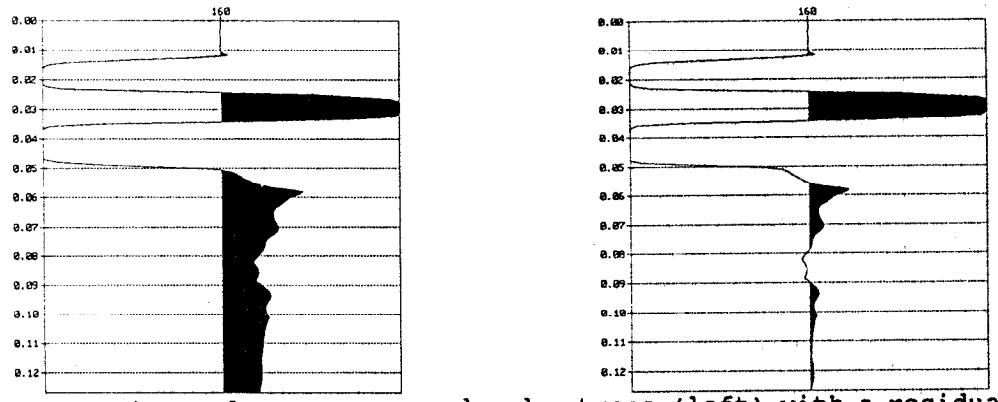

Figure 9: Comparison of an unprocessed radar trace (left) with a residual median filtered radar trace (right).

ALIGNING TIME-ZERO

"Time-zero" is the first arrival of the radar wave. For the pulseEKKO IV, it is usually found about 10% down from the start of the trace (Sensors and Software, 1987). The pre-first arrival data points are used by the pulseEKKO IV AGC and SEC gain functions to obtain a measure of the system noise. As the system components warm up, a drift of the time-zero point (generally upwards) is observed and must be corrected. This was done by manually picking the first breaks for each trace on the constant offset profiles and shifting each trace such that time-zero is aligned. The first breaks were flattened to 0.002 μs, the direct airwave traveltime for the 0.60 m antenna offset. Figure 10 shows the 100 MHz profile after wow-removal and time-zero alignment.

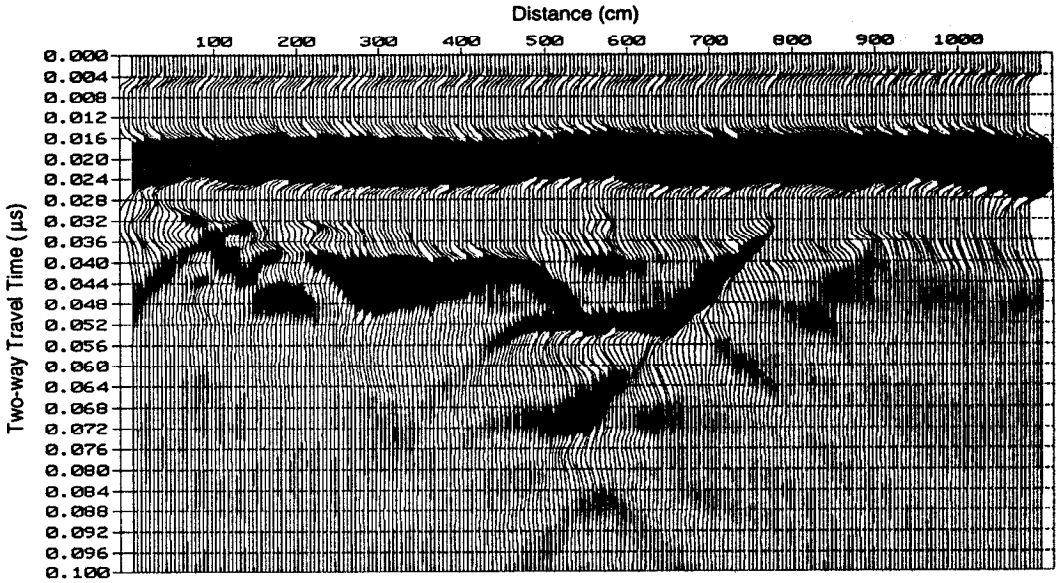

Figure 10: 100 MHz radar profile after residual median filtering and time-zero correction.

VELOCITY ANALYSIS

The GPR data were collected when the ground was thoroughly saturated. The high conductivity of the ground effectively slowed down the velocity of the EM waves such that we could better image the near-surface.

Velocity analysis was performed on the 200 MHz CMP dataset, after applying a residual median filter and correcting time-zero. Semblance analysis, a common technique in seismic processing, was implemented. Semblance analysis is based on finding the hyperbolic moveout which best fits coherent events due to primary reflections (Yilmaz, 1987).

Two RMS velocities of 68 m/μs and 61 m/μs were identified. The first RMS velocity corresponds to the saturated sand and was used in the normal moveout corrections and migration.

NORMAL MOVEOUT CORRECTIONS

Ground penetrating radar profiles are usually collected in the constant-offset ("bistatic") mode. Significant spatial distortion may result from relatively shallow depths and/or large offsets. This distortion is due to normal moveout at non-zero offsets. The normal moveout correction, which depends on both the traveltime and RMS velocity, repositions time samples to the zero-offset ("monostatic") arrival time.

For typical antenna separations, the NMO correction is minimal except for the first 0.020 μs, where the direct air and ground wave interference waveform is stretched. In seismic processing, the unaesthetic stretching of early arrivals is solved by muting out this portion (Yilmaz, 1987). However, for near surface GPR investigations, this may inadvertently destroy possible near-surface structures.

MIGRATION

The next correction that was applied was migration. The purpose of migration is to focus and reposition events to their true position in space. In the test pit images, migration effectively moved the apparent reflections to their true positions, collapsing the diffraction hyperbolas from corners and steepening the reflections from the pit walls.

ATTENUATION COMPENSATION

During data acquisition and recording, energy contained within the source wavelet is dissipated by a variety of mechanisms before it reaches the receiving antenna. Attenuation compensation attempts to recover the lost energy due to spherical divergence and attenuation of the EM signal. Seismic processing software does not have a gain function which accounts for the attenuation of EM waves. The Sensors and Software Inc. SEC exponential gain function was implemented. The data from Figure 10 are shown in Figure 11 after NMO corrections, migration and attenuation compensation.

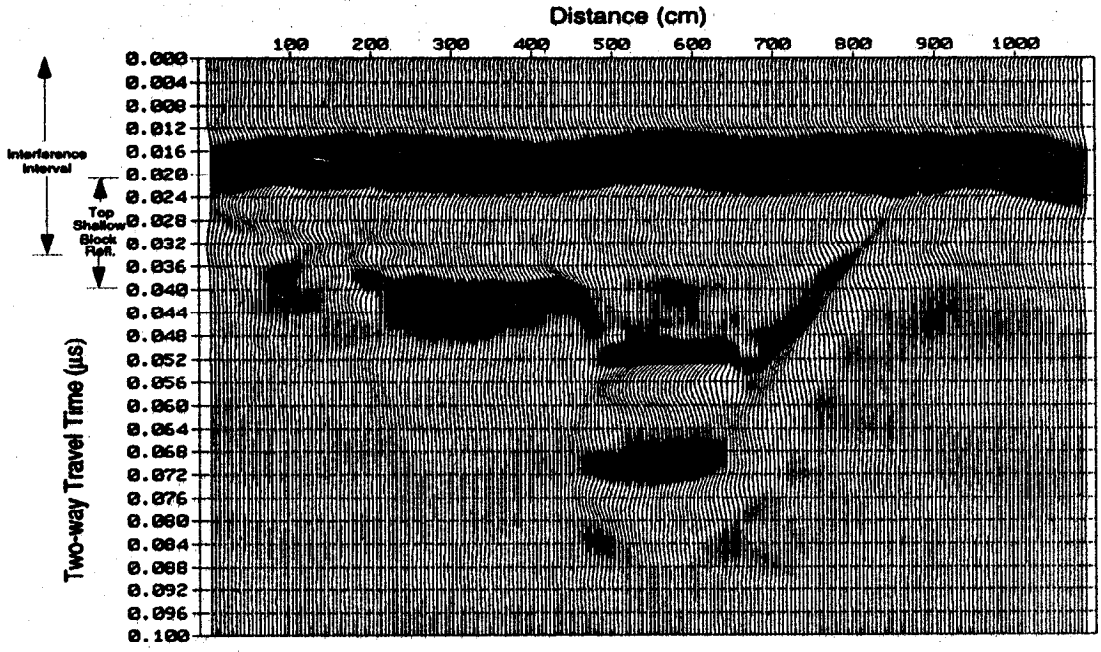

Figure 11: 100 MHz profile after NMO corrections, migration and attenuation compensation. The calculated time intervals for direct wave interference and the reflection from the top of the shallow block are labeled.

EIGEN FILTERING

A primary objective for eigen filtering is to separate direct and reflected waves. For typical antenna offsets employed in profiling configuration, direct air and ground waves interfere with one another. Additionally, this interference waveform may include a reflection from near-surface interfaces. In Figure 11 this composite response appears as very coherent amplitudes within the first 0.034 µs. Subtle yet noticeable variations of this interference response are related to near-surface structure and may be enhanced by eigen filtering.

Eigen filtering is accomplished using the singular value decomposition (SVD) of the data's covariance matrix. This precedure transforms the image into orthogonal components (the eigenimages) ordered by decreasing coherency. Details and applications of this transform are given by Jones (1985), Freire and Ulrych (1988), and applications to GPR by Luzitano (1993). Once decomposed, the image may be partially reconstructed by omitting undesired components. In particular, omitting the first eigenimage reveals the subtle variations within the coherent interference response. For a simple case, this application is equivalent to subtracting the average stacked trace. However, an important difference arises for data with laterally varying phase. To illustrate, consider two traces that differ by 180° in phase.

The stacked average results in a zero trace. However, since the SVD involves the data's covarience matrix, the lateral continuation of this signal is recognized, inspite of the polarity reversal.

Reconstructed images are compared with the original image to account for the source of the revealed features. Figure 12 illustrates the reconstructed image without the first component. This reconstruction differs from the input image (Fig. 11) primarily within the interference time interval, where most of the energy is removed. Interpretation within the interference interval remains difficult, however, since the remaining features are interference anomalies. Major differences in this reconstruction would also occur for flat continuous reflectors since they too are mostly contained in the first eigenimage. Flat discontinuous reflections, such as from the concrete blocks, are mostly contained in the second or third eigenimage. Close comparison of Figures 2, 11, and 12 reveals a correlation between the overall pattern of interference anomalies and the known near-surface structure. Undulations in the shaded lobe of the interference response appear as prominent features in the reconstructed image. The largest undulation occurs across the deepest part of the pit. Eigen filtering also reveals anomalous interference amplitudes, primarily near the pit edges. One amplitude anomaly is actually the continuation of the pit wall reflection into the interference interval. Mechanisms responsible for both the undulations and the large amplitudes near the pit edges remain speculative. Over the

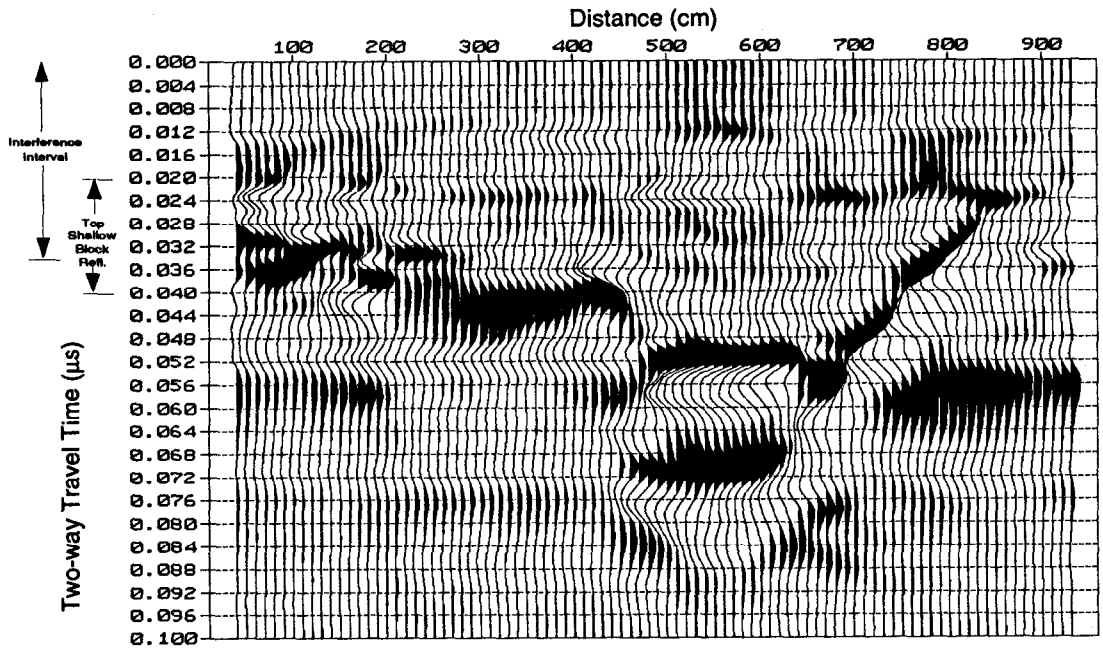

Figure 12: Eigen filtered image obtained from a reconstruction without the first component. Every other trace is shown.

shallow block, however, the reconstructed image reveals a lack of undulations where the shaded interference lobe maintains a constant delayed arrival time. This constant delay is most likely the expression of the near-surface target. The correlation between the anomaly pattern and the subsurface, as just described, is aided by examining the more simple image in Figure 13 in which the blocks appear more distinct. This second reconstructed image is composed of the second through fourth eigenimages, i.e. a bandpass in the eigenvalue sense. Although the interference interval remains difficult to interpret, eigenimage analysis does provide additional information within the interference response in the form of amplitude and timing anomalies. Although a reflection from the top of the shallow block was not resolved in the 100 MHz data, the reconstructions do reveal the detection of this block by its perturbation of the background interference response.

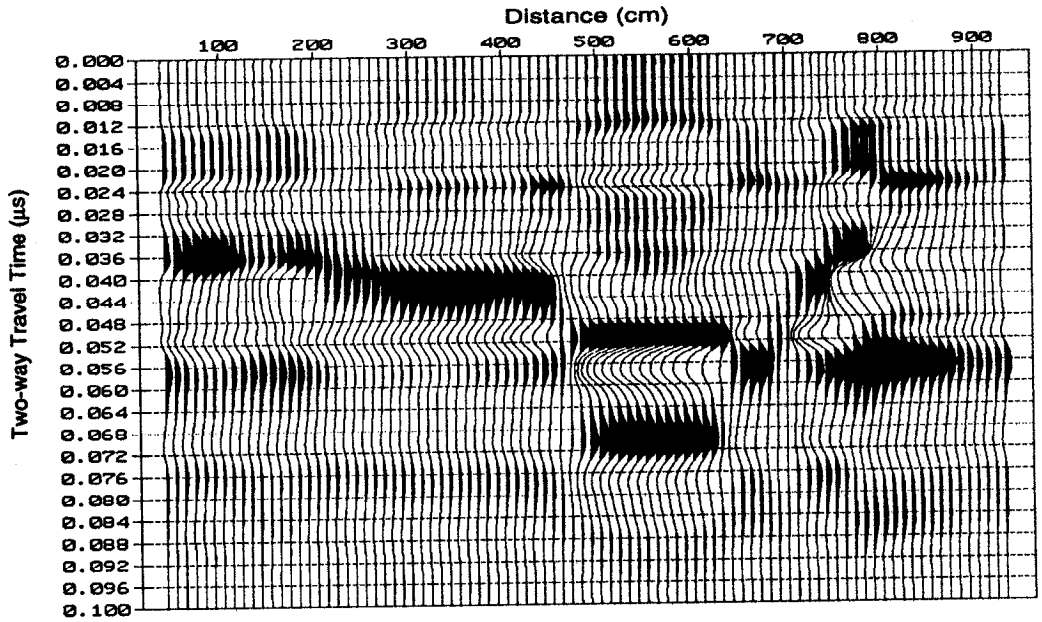

Figure 13: Image reconstructed from the second through fourth components. Every other trace is shown.

CONCLUSIONS

The application of signal processing techniques can significantly improve the quality of the GPR image, both in terms of the positioning of events and the resolving capability. By exploiting the kinematic similarities between ground penetrating radar and seismic reflection while bearing in mind some of the unique aspects of radar data, advanced signal processing of GPR data can be easily accomplished with most seismic processing software packages.

ACKNOWLEDGEMENTS

The authors are indebted to John Amor and Mike Perz for their assistance with the processing software. We would also like to thank Tad Ulrych for introducing us to eigenimage analysis.

REFERENCES

Clarke, G.K.C., Cross, G.M., and Benson, C.S., 1989, Radar imaging of glaciovolcanic stratigraphy, Mount Wrangell Caldera, Alaska: Interpretation model and results: Journal of Geophysical Research, v. 94, n. B6, p. 7237-7249.

Fisher, E., McMechan, G.A., and Annan, A.P., 1992, Acquisition and processing of wide-aperature ground-penetrating radar data: Geophysics, v. 57, n.3, p. 495-504.

Freire, S.L.M. and Ulrych, T.J., 1988, Application of singular decomposition to vertical seismic profiling: Geophysics, v. 53, n. 6, p. 778-785.

Inkster, D.R., Rossiter, J.R., Goodman, R., Galbraith, M., Davis, J.L., 1989, Ground penetrating radar data for subsurface environmental applications, *in* Seventh Thematic Conference on Remote Sensing for Exploration Geology, Calgary, Alberta, Canada, October 2-6, p.127-140.

Jones, I.F., 1985, Applications of the Karhunen-Loéve transform in reflection seismology, Ph.D. thesis, University of British Columbia, 236 p.

Luzitano, R.D., 1993, Effects of near surface structure on the GPR response, M.Sc. thesis (in preparation), University of British Columbia.

Nodes, T.A. and Gallagher, N.C., 1982, Median filters: some modifications and their properties: IEEE Transactions on Acoustics, Speech and Signal Processing, v. 30, n. 5, p. 739-746.

Sensors & Software, Inc., PulseEKKO IV User's Guide, Technical Manual 12, 86 p.

Yilmaz, O., 1987, Seismic data processing, Society of Exploration Geophysics Press, Tulsa, 526 p.